Ordering of Oxygen Vacancies and Related Ferroelectric Properties in $HfO_{2-\delta}$

Konstantin Z. Rushchanskii,* Stefan Blügel, and Marjana Ležaić
Peter Grünberg Institut and Institute for Advanced Simulation, Forschungszentrum Jülich and JARA, 52425 Jülich, Germany

(Received 26 October 2020; revised 12 May 2021; accepted 11 July 2021; published 20 August 2021)

Using density functional theory combined with an evolutionary algorithm, we investigate ferroelectricity in substoichiometric $HfO_{2-\delta}$ with fixed composition $\delta = 0.25$. We find that oxygen vacancies tend to cluster in the form of two-dimensional extended defects, revealing several patterns of local relative arrangements within an energy range of 100 meV per Hf atom. Two lowest-energy patterns result in polar monoclinic structures with different transformation properties. The lowest one elastically transforms to the ferroelectric orthorhombic structure via a shear deformation, overcoming an energy barrier, which is more than twice lower than in the stoichiometric hafnia. The second-lowest structure transforms at smaller volumes to a nonpolar tetragonal one. We discuss the experimentally observed wake-up effect, fatigue, and imprint in HfO_2-based ferroelectrics in terms of different local ordering of oxygen-vacancy extended defects, which favor specific crystallographic phases.

DOI: 10.1103/PhysRevLett.127.087602

Thin film ferroelectrics are important components of modern electronics with a wide range of applications, including nonvolatile memories, tunable microwave circuits, piezoelectric microsensors, actuators, and energy storage materials [1,2]. Development of ferroelectric films for practical applications started from the late 1960s. However, difficulties with fabrication, processing, and integration of traditional ferroelectric materials, such as $BaTiO_3$ or $PbTiO_3$, with Si devices delayed their commercial appearance till the late 1980s, when the first ferroelectric memory integrated with silicon complementary metal-oxide semiconductor (CMOS) was demonstrated [1,3]. Moreover, the issue of the critical thickness, at which the ferroelectricity disappears due to the depolarization field, as well as the existence of the "dead layers" [4], presents serious obstacles in the miniaturization of ferroelectric devices. The situation in the development of ferroelectrics-based electronics changed dramatically in 2011 after the discovery of ferroelectricity in hafnia (HfO_2) [5], which is well integrated in CMOS technology as a high-k oxide gate [6].

Bulk hafnia at room temperature and pressure adopts the nonpolar monoclinic (M) $P2_1/c$ baddeleyite structure [7]. In thin films, this phase coexists with metastable phases, such as the tetragonal (T) nonpolar fluoritelike $P4_2/nmc$ one, and the polar orthorhombic (O) phase with $Pca2_1$ symmetry [5,8–10]. Ferroelectricity in HfO_2-based thin films is induced by doping with different cations [9] like Si, Al, Gd, Sr [11], and Y [12], but it was also observed in undoped HfO_2 [13,14]. In the current view on the origin of ferroelectricity in HfO_2, the O phase is considered to carry polarity, and the switching occurs through the T phase [15,16]. Recently, ferroelectricity in (111)-oriented $Hf_{0.5}Zr_{0.5}O_2$ thin films [17] was attributed to a newly discovered polar rhombohedral phase [18]. A big surprise in comparison to the conventional ferroelectrics was the thickness dependence of the polarization, which reaches its maximum in films as thin as 10 nm [19]. This property, together with the high compatibility with state-of-the-art CMOS technology, opens new perspectives for HfO_2-based ferroelectrics as the future material of choice for high-density memory devices. Moreover, HfO_2 is also known as an active oxide for resistive switching memory devices [20,21]. Previous studies showed that resistive and ferroelectric switching mechanisms are influenced by oxygen vacancies [22]. In contrast to the resistive switching devices, where best performance is achieved in amorphous oxide layers sandwiched between asymmetric electrodes to create a gradient of oxygen vacancies, ferroelectric switching requires crystalline structure and symmetric electrodes. The coexistence of both effects was, however, recently reported [5,23]. It is noteworthy that HfO_2-based ferroelectrics are also high-capacity energy storage materials [2].

Known main problems of HfO_2-based ferroelectrics are the wake-up and fatigue effects [10]. Namely, the maximum remnant polarization is reached only after a large number of switching cycles and is accompanied by significant structural changes within the grains of the thin films. It was found that, during the wake-up phase, the fraction of M phase decreases in favor of O phase to a maximum of 80% of the volume [10]. Unfortunately, after that, the ferroelectric switching of the film enters a fatigue regime, with an increased coercive field and a decreased remnant polarization [10,24], accompanied by a further volume increase of the orthorhombic phase. Degradation of

 © 2021 American Physical Society

the ferroelectric properties is attributed to the redistribution of oxygen vacancies from the defect-rich T layer near the electrodes into the bulk, leading to a domain wall pinning [24]. Some of the pristine films also show a ferro–antiferroelectric crossover, depending on the operating temperature [25,26].

To address the role of oxygen vacancies in the ferroelectric properties of undoped HfO_2 thin films and their possible role in the problems described above, we have conducted an extensive theoretical study of the structural properties of oxygen-deficient $HfO_{2-\delta}$. Our results presented here provide a deeper understanding of the observed phenomena at the atomic scale and can serve as a guide for fabrication of high-efficiency hafnia-based ferroelectric films. We focused on a fixed composition, corresponding to the $HfO_{1.75}$ stoichiometry, and applied an evolutionary algorithm as implemented in the USPEX code [27–30] in combination with density-functional-theory calculations using the VASP code [31–33] to understand the formation of local clusters of oxygen vacancies in hafnia and the role of their ordering in elastic properties and corresponding structural transformations. Parameters used for the calculations are the same as in Ref. [34]. For more details and discussion of the role of the exchange-correlation functional on the results, see Sec. S1 in Supplemental Material [35].

We find that the low-energy structures of $HfO_{1.75}$ form four groups that are distinguished by the local oxygen vacancy arrangements. The total-energy versus volume diagrams of these groups are depicted as black, red, green, and blue lines in Fig. 1. The low-energy black and red structures show martensitic transformations within the same group. Furthermore, the structures in all considered groups are insulating (for electronic properties, see Supplemental Material, Sec. S2 [35]).

Black lines in Fig. 1 describe the structures with the vacancy ordering leading to a dielectric polarization already in the $M1$ monoclinic phase [see Fig. 2(a); crystallographic data of all discussed phases are given in Supplemental Material, Sec. S3 [35]]. The oxygen vacancies are ordered in the (100) plane of the pristine $P2_1/c$ monoclinic unit cell. Local dipoles with the largest contribution to the net polarization are located in the vicinity of oxygen vacancies. This structure transforms to the polar orthorhombic O phase [see Fig. 2(b)], which can, in fact, be seen as the oxygen-deficient $Pca2_1$ polar phase of pristine hafnia. Interphase boundaries with the orientation relations $(100)_M \| (001)_O$ and $[001]_M \| [100]_O$ for the $O \leftrightarrow M$ transition was experimentally observed in the HfO_2 grains [10]. The transformation goes via a low-energy barrier (see pathways $M1^+$—O^+ and $M1^-$—O^- in Fig. 3) of about 75 meV/Hf (per Hf atom). This barrier is almost 2.5 times lower than that at the corresponding transition to the orthorhombic phase in pristine compounds (see the dashed blue line in Fig. 3). According to our simulations, this

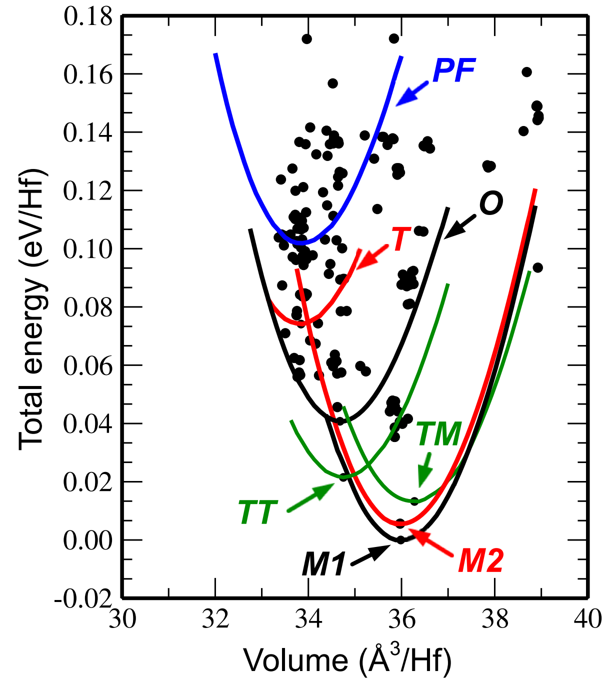

FIG. 1. Equation of state for the selected groups of crystalline structures obtained with the evolutionary algorithm: The black line corresponds to the vacancy ordering leading to the ground-state monoclinic phase $M1$ [see Fig. 2(a)], which continuously transforms to the polar orthorhombic phase O [responsible for ferroelectricity in pristine HfO_2—see Fig. 2(b)]. Red lines correspond to the vacancy ordering pattern favoring transformation of the low-energy monoclinic phase $M2$ [see Fig. 2(c)] into the nonpolar tetragonal metastable structure T [see Fig. 2(d)]. Green curves indicate intermediate phases with ordering of oxygen vacancies in tunnels in tetragonal TT and monoclinic TM hafnia [see Figs. 2(e) and 2(f)]. The blue line displays the robust $I\bar{4}2m$-Hf_4O_7 pseudo-fluorite phase PF, stemming from Hf_2O_3, which might be responsible for the resistive switching in $HfO_{2-\delta}$ (see Refs. [34,48]). Black dots indicate structures sampled by the evolutionary algorithm.

boundary is expected to show significant mobility in oxygen-deficient samples. The *in situ* observation of the mobility in the M/O interface via a shear deformation of the monoclinic angle was also reported in isostructural zirconia [49].

The polarization can be switched even within the monoclinic phase, with the energy barrier only slightly higher than that corresponding to the switching within the orthorhombic phase (compare M^+—M^- pathway in Fig. 3 with the O^+—O^- one, red line). However, this switching requires a significant shear deformation in the monoclinic phase and is not likely realized in real samples due to quenching of elastic degrees of freedom inside the grain.

Surprisingly, the switching between the monoclinic and orthorhombic phase requires a much lower energy (75 meV/Hf) comparing to the switching either solely within the orthorhombic (140 meV/Hf) or within the monoclinic (210 meV/Hf) phase (see Fig. 3).

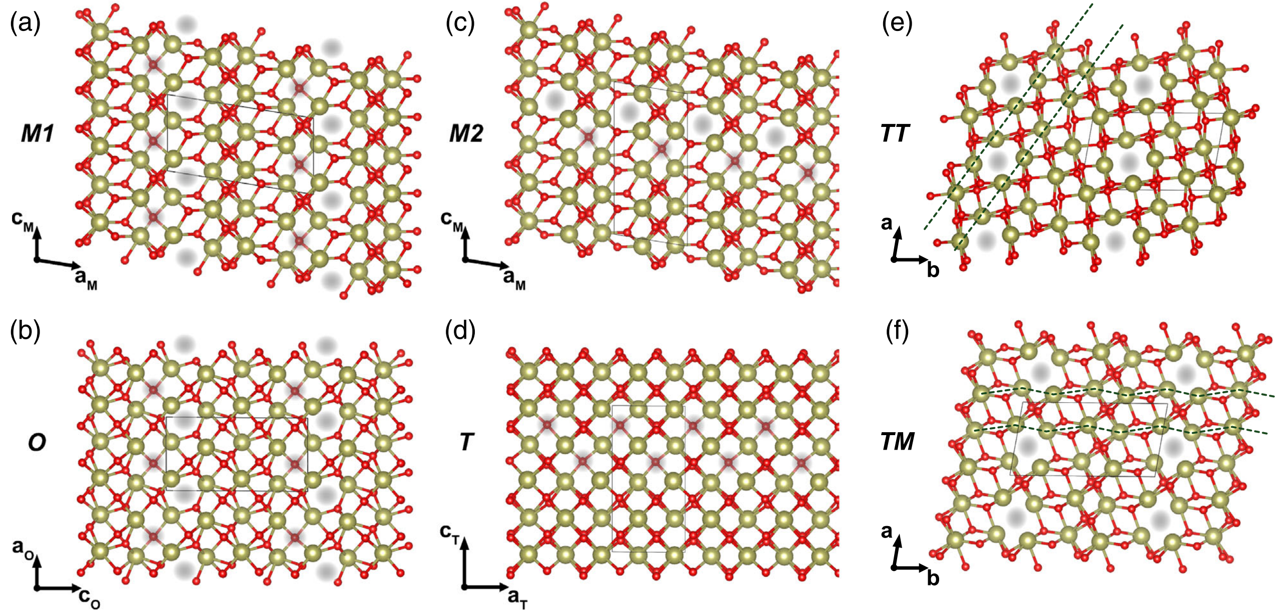

FIG. 2. Crystalline structures of the low-energy oxygen vacancy orderings in $HfO_{1.75}$: (a) monoclinic ground state $M1$ and (b) corresponding orthorhombic local minimum O of martensitic transformation along the black curve in Fig. 1; (c) second-lowest-energy monoclinic phase $M2$ and (d) corresponding martensitic tetragonal phase T along the red line in Fig. 1; (e) tunnel structure in tetragonal phase TT and (f) corresponding tunnel structure in monoclinic phase TM along the green curves in Fig. 1. Shaded areas indicate the location of oxygen vacancies. The thin solid line shows the unit cell. Hf and O atoms are shown as the big green and small red spheres, respectively. Dashed lines in (e) and (f) highlight the difference in local structural distortion for tetragonal and monoclinic structures.

We used the PSEUDO code [50] to find the centrosymmetric structures from the referenced polar $M1$ and O ones (see Supplemental Material, Sec. S4 [35]). Calculating the local displacements of ions and corresponding Born effective charges, we estimated values of the spontaneous polarization for the polar off-stoichiometric monoclinic and orthorhombic phases, as well as the change of polarization by a transformation from the monoclinic to the orthorhombic phase (see Fig. 3). We found that in the monoclinic phase itself a relatively high spontaneous polarization of $P_s = 12\ \mu\mathrm{C/cm}^2$ can be expected. In the orthorhombic phase, we obtain $P_s = 48\ \mu\mathrm{C/cm}^2$, a value similar to the one reported in the literature for the stoichiometric compound [51,52]. Switching of the monoclinic phase to the orthorhombic one results in the corresponding change of the saturated polarization value of about $P_s = 47\ \mu\mathrm{C/cm}^2$, similar to the bulk switching in the O phase.

Red lines in Fig. 1 describe the oxygen vacancy ordering with a 2D pattern in the (001) plane of the $M2$ monoclinic structure. This pattern drives the martensitic phase transition of the second-lowest-energy monoclinic structure [see Fig. 2(c)] directly to a nonpolar tetragonal T structure [compare with Fig. 2(d)]. The $M2$ structure, with this pattern of vacancies, is energetically very close to the obtained ground-state ordering of vacancies in the (100) plane of the monoclinic structure $M1$. We find that the martensitic transformation of $M2$ to the tetragonal structure results in a similar energy barrier ($\sim$71 meV/Hf) as the transformation of the $M1$ structure to the polar orthorhombic one.

Blue lines describe the elastic behavior of the PF structure, studied in detail in Ref. [48]. It is an insulating isostructural counterpart of the $Ibam$-Hf_2O_3 phase, which is a tunnel structure with metallic conductivity and low-energy migration barrier of oxygen along the tunnel [48]. In $I\bar{4}2m$-Hf_4O_7, the one-dimensional chains of oxygen vacancies are partially filled up by oxygen, resulting in an insulating state, which may explain resistive switching properties of the hafnia suboxides. This configuration of oxygen vacancies is elastically very robust, and in the considered range of volumes the structure does not transform to the low-energy monoclinic ground state, in contrast to the patterns in black and red groups. It has, however, the highest energy among the considered phases.

In addition, we also found an ordering pattern of oxygen vacancies, which results in nonpolar structures, energetically located between the orthorhombic and monoclinic phases (see green lines in Fig. 1). This ordering of vacancies is similar to the one observed in cubic phase of hafnia (which results in the $Ibam$-Hf_2O_3 phase [34,48]) and leads to structures with oxygen vacancy tunnels also in tetragonal TT and in monoclinic TM hafnia. Transformation to these configurations may activate ionic

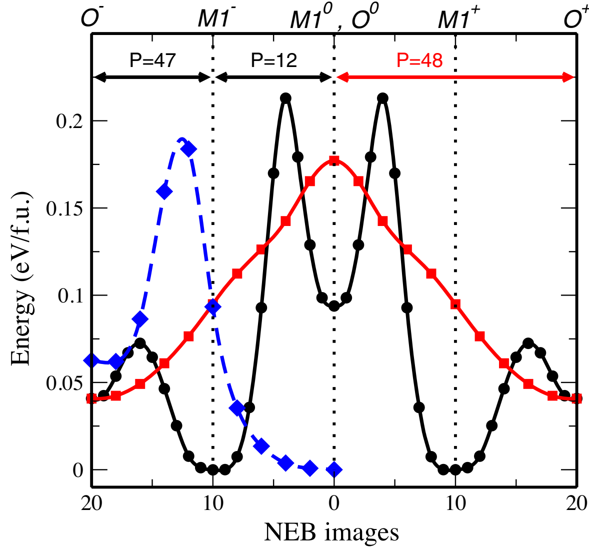

FIG. 3. Calculated energy barriers and change of spontaneous polarization along the transition path between the lowest-energy monoclinic phase $M1$ and the metastable orthorhombic phase O (black line). The O^+-to-$M1^+$ path describes the transformation between the orthorhombic and the monoclinic phase for one direction of polarization, O^- to $M1^-$, the same for the opposite direction of polarization. The path $M1^-$ to $M1^+$ describes polarization switching within the polar $M1$ phase. Ferroelectric switching within the orthorhombic phase (without the $O-M1$ transformation) follows the $O^- - O^0 - O^+$ path shown in red. The blue dashed line describes the transition from the monoclinic to the orthorhombic phase in *stoichiometric* hafnia. Numbers above the arrows are differences of polarization P in the corresponding parts of the transformation path (in $\mu C/cm^2$).

conductivity and resistive switching properties in the sample [34,48], but stabilization of the nonpolar phases may cause degradation of the ferroelectric properties of $HfO_{2-\delta}$.

Another mechanism of degradation of the ferroelectric properties may lie in the oxidation of the thin film by atmospheric oxygen, leading back to stoichiometric hafnia. As is shown in Fig. 3, the energy barrier for the $O \leftrightarrow M$ transition in stoichiometric films increases significantly, leading to a rise of the coercive field. From a more constructive point of view, however, the oxidation of the films may be used for stabilization of the orthorhombic phase after transforming the monoclinic one to the polar O phase in oxygen-deficient films.

Next, we discuss, in light of our findings, some details of the previously mentioned experimental observations and issues in hafnia-based ferroelectrics. Namely, it was recently experimentally demonstrated [22,53,54] that during the wake-up of the device no new defects are generated, but the existing defects redistribute within the device. In Refs. [22,54], in stacks with asymmetrical electrodes, valence change resistive switching was observed together with ferroelectric switching.

We conjecture that, during the wake-up cycles, randomly distributed oxygen vacancies are reordered to the lowest-energy configuration, enabling the switching to the orthorhombic phase and preventing a transformation to the nonpolar tetragonal one. In addition to electron-injection-assisted generation [55] and consequent aggregation [56] of oxygen vacancies, their ordering in 2D planes might be achieved by elastic gradients in the moving interphase boundary due to lattice mismatch of the monoclinic and higher-symmetry phases. After the redistribution of the vacancies, the monoclinic phase is transformed via the low-energy barrier to the orthorhombic one. The monoclinic phase can be seen as a domain boundary between the orthorhombic domains with opposite polarization (or vice versa, depending on the relative amount of phases). An increase of polarization might be not due to the bulk polarization switching within the orthorhombic phase itself but due to the growth of the orthorhombic phase on the boundary of the monoclinic one. A decrease of the polarization might be either a reversal transformation of the orthorhombic phase back to the monoclinic one or by the growth of the orthorhombic phase with the opposite direction of polarization. In the latter case, the ratio of the monoclinic phase gradually decreases during the switching cycles, and at the end only the metastable orthorhombic phase remains. After that, ferroelectric switching occurs in the orthorhombic phase only, with a higher transition barrier (see the O^-—O^+ pathway in Fig. 3), which results in an increase of the coercive field. This picture might explain the experimentally observed decrease of the amount of the monoclinic phase in initially prepared samples and the growth of the O one [10].

The switching mechanism, which involves the presence of the monoclinic phase, naturally explains the experimentally observed imprint effect [57], with shifted origin of the hysteresis loop: In the presence of vacancies, the monoclinic phase is polar with a high switching barrier. The high barrier prevents switching within the monoclinic phase, but its polarity acts as an electrostatic background that shifts the hysteresis loop, which itself arises from the switching by the growth of the orthorhombic phase on the monoclinic boundary or from the bulk switching within the orthorhombic phase.

Furthermore, the observed temperature crossover from ferroelectric to antiferroelectric behavior [25,26] might be explained in the proposed scheme: The transition barrier between the orthorhombic and monoclinic phase is asymmetric; therefore, at high temperature, the orthorhombic phase may easily return to the monoclinic one by thermal fluctuations when the external electric field is removed, leading to the antiferroelectriclike shape of the hysteresis loop. At low temperature, the orthorhombic phase is quenched after the removal of the external field, holding the remnant polarization close to the saturated one.

The vacancy concentration of $x = 1.75$ used in our calculations is rather the upper limit when the defective structure is not stabilized in the cubic form and the low-energy structures are still insulating [34,48] and have the same set of structural modifications (monoclinic, orthorhombic, tetragonal, and cubic) as the stoichiometric compound. The clustering of the vacancies in the planes defines the criterion for their minimum concentration to enable the proposed mechanism: The plane is expected to cross the grain. In ideally ordered configurations, the actual concentration of vacancies defines the distance between the planes. We might then expect gradual changes in the transition barrier as a function of the interplane distance where its maximum reaches in the stoichiometric hafnia.

In conclusion, at normal conditions, oxygen vacancies in the bulk material do not lead to the stabilization of the O phase, as, e.g., in the case of ordered Si dopants [58]. However, we show that the presence of a limited number of oxygen vacancies in hafnia results in a polar structure already in the monoclinic phase. We found two clustering patterns of the oxygen vacancies, which are almost degenerate energetically but define different pathways of the martensitic phase transition from the monoclinic phase to the polar orthorhombic or to the nonpolar tetragonal structures. These results are applicable for similar transformations in isostructural zirconia [59,60]. We discussed a possible mechanism of ferroelectric switching, which involves a transition between the O and M phases. Between the ground-state monoclinic and the metastable orthorhombic phases, we found tunnel structures, which favor ionic conductivity and may cause degradation of ferroelectric properties. The switching pathways we discussed here naturally manifest themselves in the experimentally observed phenomena, such as the existence of the wake-up and fatigue regimes as well as the imprint effect, providing credibility to the proposed switching mechanism.

We gratefully acknowledge the financial support by Deutsche Forschungsgemeinschaft (DFG) through SFB 917 “Nanoswitches,” as well as the computing time granted by the Jülich-Aachen Research Alliance (JARA) Vergabegremium and provided on the JARA Partition part of the supercomputer JURECA [61] at Forschungszentrum Jülich and JARA-HPC Partition (Project No. jara0126). Visualization was made with the help of the VESTA code [62]. The FINDSYM package [63] was used for symmetry analysis of obtained structures. We thank Dr. Ivetta Slipukhina for the critical reading of the manuscript and valuable suggestions.

*Corresponding author.
k.rushchanskii@fz-juelich.de

[1] N. Setter, D. Damjanovic, L. Eng, G. Fox, S. Gevorgian, S. Hong, A. Kingon, H. Kohlstedt, N. Y. Park, G. B. Stephenson, I. Stolitchnov, A. K. Taganstev, D. V. Taylor, T. Yamada, and S. Streiffer, J. Appl. Phys. **100**, 051606 (2006).
[2] F. Ali, X. Liu, D. Zhou, X. Yang, J. Xu, T. Schenk, J. Müller, U. Schroeder, F. Cao, and X. Dong, J. Appl. Phys. **122**, 144105 (2017).
[3] S. S. Eaton, D. B. Butler, M. Parris, D. Wilson, and H. McNeillie, *IEEE International Solid-State Circuits Conference, 1988 ISSCC. Digest of Technical Papers, San Francisco, CA, USA* (1988), pp. 130–131, https://ieeexplore.ieee.org/document/663665.
[4] M. Stengel, D. Vanderbilt, and N. A. Spaldin, Nat. Mater. **8**, 392 (2009).
[5] T. S. Böscke, J. Müller, D. Bräuhaus, U. Schröder, and U. Böttger, Appl. Phys. Lett. **99**, 102903 (2011).
[6] Z. Fan, J. Chen, and J. Wang, J. Adv. Dielectr. **06**, 1630003 (2016).
[7] R. N. Patil and E. C. Subbarao, J. Appl. Crystallogr. **2**, 281 (1969).
[8] X. Sang, E. D. Grimley, T. Schenk, U. Schroeder, and J. M. LeBeau, Appl. Phys. Lett. **106**, 162905 (2015).
[9] M. H. Park, T. Schenk, C. M. Fancher, E. D. Grimley, C. Zhou, C. Richter, J. M. LeBeau, J. L. Jones, T. Mikolajick, and U. Schroeder, J. Mater. Chem. C **5**, 4677 (2017).
[10] E. D. Grimley, T. Schenk, T. Mikolajick, U. Schroeder, and J. M. LeBeau, Adv. Mater. Interfaces **5**, 1701258 (2018).
[11] T. Schenk, S. Mueller, U. Schroeder, R. Materlik, A. Kersch, M. Popovici, C. Adelmann, S. Van Elshocht, and T. Mikolajick, in *Proceedings of the European Solid-State Device Research Conference (ESSDERC), 2013* (IEEE, New York, 2013), pp. 260–263.
[12] J. Müller, U. Schröder, T. S. Böscke, I. Müller, U. Böttger, L. Wilde, J. Sundqvist, M. Lemberger, P. Kücher, T. Mikolajick, and L. Frey, J. Appl. Phys. **110**, 114113 (2011).
[13] P. Polakowski and J. Müller, Appl. Phys. Lett. **106**, 232905 (2015).
[14] T. Mittmann, M. Materano, P. D. Lomenzo, M. H. Park, I. Stolichnov, M. Cavalieri, C. Zhou, C.-C. Chung, J. L. Jones, T. Szyjka, M. Müller, A. Kersch, T. Mikolajick, and U. Schroeder, Adv. Mater. Interfaces **6**, 1900042 (2019).
[15] S. E. Reyes-Lillo, K. F. Garrity, and K. M. Rabe, Phys. Rev. B **90**, 140103(R) (2014).
[16] S. V. Barabash, D. Pramanik, Y. Zhai, B. Magyari-Kope, and Y. Nishi, ECS Trans. **75**, 107 (2017).
[17] S. Starschich, T. Schenk, U. Schroeder, and U. Boettger, Appl. Phys. Lett. **110**, 182905 (2017).
[18] Y. Wei, P. Nukala, M. Salverda, S. Matzen, H. J. Zhao, J. Momand, A. S. Everhardt, G. Agnus, G. R. Blake, P. Lecoeur, B. J. Kooi, J. Íñiguez, B. Dkhil, and B. Noheda, Nat. Mater. **17**, 1095 (2018).
[19] X. Tian, S. Shibayama, T. Nishimura, T. Yajima, S. Migita, and A. Toriumi, Appl. Phys. Lett. **112**, 102902 (2018).
[20] M. Lanza *et al.*, Adv. Electron. Mater. **5**, 1800143 (2019).
[21] L. Goux, P. Czarnecki, Y. Y. Chen, L. Pantisano, X. P. Wang, R. Degraeve, B. Govoreanu, M. Jurczak, D. J. Wouters, and L. Altimime, Appl. Phys. Lett. **97**, 243509 (2010).
[22] S. Starschich, S. Menzel, and U. Böttger, Appl. Phys. Lett. **108**, 032903 (2016).
[23] B. Max, M. Pešić, S. Slesazeck, and T. Mikolajick, J. Appl. Phys. **123**, 134102 (2018).

[24] E. D. Grimley, T. Schenk, X. Sang, M. Pešić, U. Schroeder, T. Mikolajick, and J. M. LeBeau, Adv. Electron. Mater. **2**, 1600173 (2016).

[25] M. H. Park, C.-C. Chung, T. Schenk, C. Richter, M. Hoffmann, S. Wirth, J. L. Jones, T. Mikolajick, and U. Schroeder, Adv. Electron. Mater. **4**, 1700489 (2018).

[26] M. H. Park and C. S. Hwang, Rep. Prog. Phys. **82**, 124502 (2019).

[27] A. R. Oganov and C. W. Glass, J. Chem. Phys. **124**, 244704 (2006).

[28] A. R. Oganov, A. O. Lyakhov, and M. Valle, Acc. Chem. Res. **44**, 227 (2011).

[29] A. O. Lyakhov, A. R. Oganov, H. T. Stokes, and Q. Zhu, Comput. Phys. Commun. **184**, 1172 (2013).

[30] A. R. Oganov, Y. Ma, A. O. Lyakhov, M. Valle, and C. Gatti, Rev. Mineral. Geochem. **71**, 271 (2010).

[31] G. Kresse and J. Hafner, Phys. Rev. B **47**, 558 (1993).

[32] G. Kresse and J. Furthmüller, Phys. Rev. B **54**, 11169 (1996).

[33] G. Kresse and D. Joubert, Phys. Rev. B **59**, 1758 (1999).

[34] K. Z. Rushchanskii, S. Blügel, and M. Ležaić, Faraday Discuss. **213**, 321 (2019).

[35] See Supplemental Material at http://link.aps.org/supplemental/10.1103/PhysRevLett.127.087602 for supporting content, which includes Refs. [36–47].

[36] R. Martoňák, A. Laio, and M. Parrinello, Phys. Rev. Lett. **90**, 075503 (2003).

[37] P. E. Blöchl, Phys. Rev. B **50**, 17953 (1994).

[38] J. P. Perdew, K. Burke, and M. Ernzerhof, Phys. Rev. Lett. **77**, 3865 (1996).

[39] S. L. Dudarev, G. A. Botton, S. Y. Savrasov, C. J. Humphreys, and A. P. Sutton, Phys. Rev. B **57**, 1505 (1998).

[40] D. Sangalli and A. Debernardi, Phys. Rev. B **84**, 214113 (2011).

[41] C. Carbogno, C. G. Levi, C. G. Van de Walle, and M. Scheffler, Phys. Rev. B **90**, 144109 (2014).

[42] H. Shin, A. Benali, Y. Luo, E. Crabb, A. Lopez-Bezanilla, L. E. Ratcliff, A. M. Jokisaari, and O. Heinonen, Phys. Rev. Mater. **2**, 075001 (2018).

[43] G. I. Csonka, J. P. Perdew, A. Ruzsinszky, P. H. T. Philipsen, S. Lebègue, J. Paier, O. A. Vydrov, and J. G. Ángyán, Phys. Rev. B **79**, 155107 (2009).

[44] J. Sun, A. Ruzsinszky, and J. P. Perdew, Phys. Rev. Lett. **115**, 036402 (2015).

[45] A. V. Krukau, O. A. Vydrov, A. F. Izmaylov, and G. E. Scuseria, J. Chem. Phys. **125**, 224106 (2006).

[46] A. D. Becke, J. Chem. Phys. **98**, 5648 (1993).

[47] P. J. Stephens, F. J. Devlin, C. F. Chabalowski, and M. J. Frisch, J. Phys. Chem. **98**, 11623 (1994).

[48] K. Z. Rushchanskii, S. Blügel, and M. Ležaić, Phys. Rev. Mater. **2**, 115002 (2018).

[49] Y.-H. Chiao and I.-W. Chen, Acta Metall. Mater. **38**, 1163 (1990).

[50] C. Capillas, E. S. Tasci, G. de la Flor, D. Orobengoa, J. M. Perez-Mato, and M. I. Aroyo, Z. Kristallogr. Cryst. Mater. **226**, 186 (2011).

[51] M. Pešić, C. Künneth, M. Hoffmann, H. Mulaosmanovic, S. Müller, E. T. Breyer, U. Schroeder, A. Kersch, T. Mikolajick, and S. Slesazeck, J. Comput. Electron. **16**, 1236 (2017).

[52] P. Fan, Y. K. Zhang, Q. Yang, J. Jiang, L. M. Jiang, M. Liao, and Y. C. Zhou, J. Phys. Chem. C **123**, 21743 (2019).

[53] M. Pei, F. P. G. Fengler, L. Larcher, A. Padovani, T. Schenk, E. D. Grimley, X. Sang, J. M. LeBeau, S. Slesazeck, U. Schroeder, and T. Mikolajick, Adv. Funct. Mater. **26**, 4601 (2016).

[54] S. Starschich, S. Menzel, and U. Böttger, J. Appl. Phys. **121**, 154102 (2017).

[55] S. R. Bradley, A. L. Shluger, and G. Bersuker, Phys. Rev. Applied **4**, 064008 (2015).

[56] S. R. Bradley, G. Bersuker, and A. L. Shluger, J. Phys. Condens. Matter **27**, 415401 (2015).

[57] F. P. G. Fengler, M. Hoffmann, S. Slesazeck, T. Mikolajick, and U. Schroeder, J. Appl. Phys. **123**, 204101 (2018).

[58] S. Dutta, H. Aramberri, T. Schenk, and J. Íñiguez, Phys. Status Solidi **14**, 2000047 (2020).

[59] G. Trolliard, D. Mercurio, and J. Perez-Mato, Z. Kristallogr. Cryst. Mater. **226**, 264 (2011).

[60] S.-H. Guan, X.-J. Zhang, and Z.-P. Liu, J. Am. Chem. Soc. **137**, 8010 (2015).

[61] Jülich Supercomputing Centre, J. Large-Scale Res. Facil. **4**, A132 (2018).

[62] K. Momma and F. Izumi, J. Appl. Crystallogr. **44**, 1272 (2011).

[63] H. T. Stokes and D. M. Hatch, J. Appl. Crystallogr. **38**, 237 (2005).